

The mesoscopic conductance of ballistic rings

Yoav Etzioni, Swarnali Bandopadhyay[‡] and Doron Cohen

Department of Physics, Ben-Gurion University, Beer-Sheva 84005, Israel

Abstract. The calculation of the conductance of ballistic rings requires a theory that goes well beyond the Kubo-Drude formula. Assuming “mesoscopic” circumstance of very weak environmental relaxation, the conductance is much smaller compared with the naive expectation. Namely, the electro-motive-force induces an energy absorption with a rate that depends crucially on the possibility to make connected sequences of transitions. Thus the calculation of the mesoscopic conductance is similar to solving a percolation problem. The “percolation” is in energy space rather than in real space. Non-universal structures and sparsity of the perturbation matrix cannot be ignored. The latter are implied by lack of quantum-chaos ergodicity in ring shaped ballistic devices.

1. Introduction

Closed mesoscopic rings are of great interest [1-13]. For such devices the relation between the conductance and the internal dynamics is understood much less [14, 15] than for open systems. First measurements of the conductance of closed mesoscopic rings have been reported more than a decade ago [13]. In a typical experiment a collection of mesoscopic rings is driven by a time dependent magnetic flux $\Phi(t)$ which creates an electro-motive-force (EMF) $-\dot{\Phi}$ in each ring. Assuming that Ohm’s law applies, the induced current is $\mathcal{I} = -G\dot{\Phi}$ and consequently the rate of energy absorption is given by Joule’s law as

$$\dot{\mathcal{W}} = \text{Rate of energy absorption} = G\dot{\Phi}^2 \quad (1)$$

where G is called the conductance \S . For diffusive rings the Kubo formalism leads to the Drude formula for G . A major challenge in past studies was to calculate the weak localization corrections to the Drude result, taking into account the level statistics and the type of occupation [12]. It should be clear that these corrections do not challenge the leading order Kubo-Drude result.

Theoretical challenge: It is just natural to ask [14, 15] what happens to the Drude result if the disorder becomes weak (ballistic case) or strong (Anderson localization case). In both cases the individual eigenfunctions become non ergodic: a typical eigenfunction do not fill the whole accessible phase space. In the ballistic case a typical eigenfunction is not ergodic over the open modes in momentum space, while

[‡] Present address: Max Planck Institute for the Physics of Complex Systems, Nöthnitzer Str. 38, 01187 Dresden, Germany

[§] The terminology of this paper, and in particular our notion of “conductance” are the same as in the theoretical review [12] and in the experimental work [13].

in the strong localization case it is not ergodic over the ring in real space.

Major observation: Lack of quantum ergodicity implies that the perturbation matrix is very structured and/or sparse. Consequently the calculation of G requires a non-trivial extension of linear response theory (LRT). Such extension has been proposed in Ref.[15] and later termed “semi linear response theory” (SLRT) [16, 17]. As in the standard derivation of the Kubo formula, also within the framework of SLRT, the leading mechanism for absorption is assumed to be Fermi-golden-rule (FGR) transitions. These are proportional to the squared matrix elements $|\mathcal{I}_{nm}|^2$ of the current operator. Still, the theory of [15] does not lead to the Kubo formula. This is because the rate of absorption depends crucially on the possibility to make *connected* sequences of transitions, and it is greatly reduced by the presence of bottlenecks. It is implied that both the structure of the $|\mathcal{I}_{nm}|^2$ band profile and its sparsity play a major role in the calculation of G .

SLRT and beyond: Within SLRT it is assumed that the transitions between levels are given by Fermi-golden-rule, but a resistor network analogy [18] is used in order to calculate the overall absorption. The calculation of the energy absorption in Eq.(1) is somewhat similar to solving a percolation problem. The “percolation” is in energy space rather than in real space. A recent study [19] suggests a way to go beyond the FGR approximation. If the results of Ref [19] could be extended beyond the diffusive regime [20] it would be possible to extend SLRT into the non-linear regime.

Scope: In a follow up work [21] it is demonstrated that for a very strong disorder SLRT leads naturally to the resistor network “hopping” picture [22, 23], from which Mott’s variable-range-hopping approximation [24, 25] can be derived. In the present work we apply SLRT to the other extreme case, of having a ballistic ring. It should be appreciated that the generalized resistor network picture of SLRT provides a firm unified framework for the calculation of the mesoscopic conductance: The same recipe is used in both extreme cases without the need to rely on an ad-hock phenomenology.

Ballistic rings: In the case of a diffusive rings the mean free path ℓ is assumed to be much less than the perimeter L of the ring. In the case of ballistic ring we have the opposite situation $\ell \gg L$. One way to model a ballistic ring is to consider very weak disorder (Fig. 1a). Another possibility is to consider a clean ring with a single scatterer (Fig. 1b) or a small deformation (Fig. 1c). In the latter cases it is natural to characterize the scattering region by its total transmission $g_T \sim 1$. Consequently the mean free path is

$$\ell \approx \frac{1}{1 - g_T} L \quad (2)$$

The assumption of ballistic motion implies that “quantum chaos” considerations are important. Consequently one should go well beyond the conventional random wave picture of Mott [24, 25], and beyond the standard Random Matrix Theory analysis. In fact we are going to explain that in this limit the eigenfunctions are non-ergodic, and hence the perturbation matrix $|\mathcal{I}_{nm}|^2$ is structured and sparse.

Outline: The purpose of this paper is to discuss the modeling of ballistic rings; to clarify the procedure which is involved in the calculation of the conductance; and to analyze the simplest example. In sections 2 we distinguish between

- Disordered rings (e.g. Anderson model)
- Chaotic rings (e.g. billiard systems)
- Network models (also known as “graphs”)

These are illustrated in Fig. 1. In particular we motivate the analysis of a simple prototype network model for a multimode ring. This model has all the essential ingredients to demonstrate the major theme of this paper.

In sections 3-8 we elaborate on the procedure which is used for the calculation of the conductance. This is not merely a technical issue, since new concepts [15, 17] are involved. We make a distinction between:

- The Landauer result for the open device
- The classical Drude result for a closed ring
- The (quantum) spectroscopic conductance of a ring
- The (quantum) mesoscopic conductance of a ring

Here “classical” as opposed to “quantum” should be understood in the sense of Boltzmann picture. In the “classical” case the interference within the arm of the ring is ignored, while both the Fermi statistics and the single scattering events are treated properly. For the prototype model we get the following simple results: Given that the device has \mathcal{M} open modes and its total transmission is $g_T < 1$, the Landauer conductance is [26]

$$G_{\text{Landauer}} = \frac{e^2}{2\pi\hbar} \mathcal{M} g_T \quad (3)$$

The Drude result for the closed ring is

$$G_{\text{Drude}} = \frac{e^2}{2\pi\hbar} \mathcal{M} \frac{g_T}{1 - g_T} \quad (4)$$

and the associated quantum results are

$$G_{\text{spec}} \approx \frac{e^2}{2\pi\hbar} \mathcal{M} \times \text{minimum} \left[\frac{g_T}{1 - g_T}, \mathcal{M} \right] \quad (5)$$

$$G_{\text{meso}} = \frac{e^2}{2\pi\hbar} 2\mathcal{M}^2 g_{\text{meso}} \quad (6)$$

The calculation of g_{meso} involves a complicated *coarse graining* procedure that we discuss in section 8. The spectroscopic result G_{spec} describes via Eq.(1) both the initial (transient) rate and also the long time (steady state) rate of energy absorption, provided the environment provides a strong relaxation mechanism. The mesoscopic result describes the (slower) long time rate of energy absorption if the environmentally induced relaxation is weak. See [15] for an extended quantitative discussion.

The outcome for G_{meso} may differ by orders of magnitude from the conventional Kubo-Drude result. The calculation procedure implies that $G_{\text{meso}} < G_{\text{spec}} \leq G_{\text{Drude}}$. In the last part of this paper (sections 9-12) we demonstrate this point via the analysis of the prototype model. Our numerical results, whose preliminary version were reported in [27], suggest that typically $G_{\text{meso}} < G_{\text{Landauer}}$. The results of the calculation are contrasted with those of the conventional Kubo approach, and their *robustness* is discussed.

2. Modeling

A simple model for a ballistic ring can be either of the “disordered type” or of the “chaotic type”. Let us visualize the disordered potential as arising from a set of scatterers which are distributed all over the ring (Fig 1a). Depending on the scattering cross section of the individual scatterers we can have $\ell \ll L$ for strong disorder or $\ell \gg L$ for weak disorder, where ℓ is the mean free path for velocity randomization, and L is the perimeter of the ring.

Another possibility is not to make all the scatterers smaller, but rather to dilute them. Eventually we may have a chaotic ring where the scattering is induced by a single scatterer (Fig 1b). For example the scatterer can be a disc or a semi-disc as in Fig 2. These variations of Sinai billiard (billiard with convex wall elements) are known to be chaotic. It is important to remember that “chaos” means that complicated ergodic classical dynamic is generated by a simple Hamiltonian (*no disorder!*).

In our view chaotic rings are more interesting for various reasons. Ballistic devices are state-of-art in mesoscopic experiments. For example it is quite common to fabricate Aharonov-Bohm devices. In such devices it is possible to induce local deformation of the potential by means of a gate voltage. Hence one has a full control over the amount of scattering. Also from theoretical point of view it is nice to have a well defined scattering region: This allows to use the powerful S -matrix point of view that has been initiated by Landauer. In particular we can ask what is the conductance of a device depending on whether it is integrated in an open geometry as in Fig. 1e or in a closed geometry as in Fig. 1d. We believe that “chaos” and “disorder” lead to similar physics in the present context, but this claim goes beyond the scope of the present paper.

A multimode ring can be visualized as a waveguide of length L and width W . In such case the number of open modes is $\mathcal{M} \propto (k_F W)^{d-1}$ where $d = 2, 3$ is the dimensionality. We label the modes as

$$a = \text{mode index} = 1, 2, \dots, \mathcal{M} \quad (7)$$

The scattering arise due to some bump or some deformation of the boundary, and can be described by an $2\mathcal{M} \times 2\mathcal{M}$ scattering matrix \mathcal{S} . For the semi-disc model analytical complicated expressions are available [29, 30]. The “classical” transitions probability matrix \mathbf{g} is obtained by squaring the absolute values of the \mathcal{S} matrix elements.

Disregarding the closed channels, the ballistic ring is described as a set of \mathcal{M} open modes, and a small scattering region that is characterized by its total transmission g_T . Optionally the ballistic ring can be regarded as a network: Each bond corresponds to an open mode. Let us consider the simplest model where the scattering is the same for an incident particle that comes from the left or from the right:

$$\mathbf{g} = \begin{pmatrix} [\mathbf{g}^R]_{a,b} & [\mathbf{g}^T]_{a,b} \\ [\mathbf{g}^T]_{a,b} & [\mathbf{g}^R]_{a,b} \end{pmatrix} \quad (8)$$

where \mathbf{g}^R is the reflection matrix and \mathbf{g}^T is the transmission matrix. The simplest model that one can imagine is with

$$[\mathbf{g}^R]_{a,b} = \epsilon^2 \quad (9)$$

$$[\mathbf{g}^T]_{a,b} = (1 - \mathcal{M}\epsilon^2)\delta_{a,b} \quad (10)$$

such that the total transmission is

$$g_T = 1 - \mathcal{M}\epsilon^2 \quad (11)$$

Such “classical” transitions probability matrix can arise if we take the S matrix as

$$\mathbf{S}_D = \begin{pmatrix} \epsilon \exp\left(i 2\pi \frac{a b}{\mathcal{M}}\right) & \sqrt{1 - \mathcal{M}\epsilon^2} \delta_{a,b} \\ \sqrt{1 - \mathcal{M}\epsilon^2} \delta_{a,b} & -\epsilon \exp\left(-i 2\pi \frac{a b}{\mathcal{M}}\right) \end{pmatrix} \quad (12)$$

There a lot of simplifications that were involved in construction this \mathbf{S} matrix.

- The forward scattering is to the same mode only
- The back scattering is “isotropic”
- The scattering is energy independent
- The scattering phases are not random

One can wonder whether this \mathbf{S} matrix still qualifies as ‘generic’, or maybe the model is over-simplistic. In order to illuminate this point let us look at the Sinai billiard models of Fig. 2. These models are fully qualified as “quantum chaos” systems. One observes that the specific \mathbf{g} matrix of Eq.(9-10) is inspired by that of Fig. 2a. In this billiard an incident particle is equally likely to be scattered to any mode in the backward direction, but the forward scattering is only to the same mode (same angle). As for the phases: we already have explained that our interest is not in disordered ring, but rather in chaotic one. Therefore to have random phases in the \mathbf{S} matrix is not an essential feature of the model. The phases are effectively randomized simply because the wavenumber k_a is different in each mode. Optionally, it is more convenient to assume that all the k_a are equal, and instead to have bonds of different lengths L_a . This provides the required phase randomization.

Generality: Though the arguments above strongly suggest that the simplified network model is generic, we were careful to verify [28] that indeed all the results that we find are also applicable in the case of the Sinai-type system of Fig. 2b where the scatterer is a semi-disc. We further discuss the *robustness* of the results in the concluding section. Sinai-type billiards are recognized as generic chaotic systems. The reason for preferring the network model as the leading example in the present paper is both pedagogical and practical: The mathematics is much simpler, and the quality of the numerics is much better.

3. The classical Kubo formula and Drude

The Fluctuation-Dissipation version of the Kubo formula expresses the conductance G as an integral over the current-current correlation function:

$$G = \varrho_F \times \frac{1}{2} \int_{-\infty}^{\infty} \langle \mathcal{I}(t) \mathcal{I}(0) \rangle dt \quad (13)$$

The density of states at the Fermi energy is

$$\varrho_F = \text{GeometricFactor} \times \mathcal{M} \frac{L}{\pi \hbar v_F} \quad (14)$$

where v_F is the Fermi velocity. The geometric factor depends on the dimensionality $d = 1, 2, 3$. The current observable is defined as follows:

$$\mathcal{I} = e \hat{v} \delta(\hat{x} - x_0) \quad (15)$$

where \hat{v} and \hat{x} are the velocity and the position observables respectively. In the quantum case a symmetrization of this expression is required, so as to obtain an hermitian operator. The section through which the current is measured is arbitrary and we simply take $x_0 = +0$, namely just to the right of the scattering region.

Optionally, if there were not the “black box” region of the \mathbf{S} matrix, one could average over x_0 , leading to $\mathcal{I} = (e/L)v$.

The term “classical” Kubo formula implies in this context that the current-current correlation function is evaluated classically, ignoring quantum interference. In the case of hard chaos system this correlation function decays exponentially. The Drude expression is the simplest classical approximation:

$$\langle \mathcal{I}(t)\mathcal{I}(0) \rangle = \frac{1}{d} \left(\frac{e}{L} v_F \right)^2 \exp \left[-2 \left(\frac{v_F}{\ell} \right) |t| \right] \quad (16)$$

Substitution into the Kubo formula leads to

$$G_{\text{Drude}} = \frac{e^2}{2\pi\hbar} \mathcal{M} \frac{\ell}{L} \quad (17)$$

where we have dropped the d dependent prefactor which equals 1 for networks ($d = 1$). In the case of a ballistic ring with a restricted scattering region (as in Fig. 1d) it is more convenient to characterize the device by its total transmission $0 < g_T < 1$ instead of the mean free path. The envelope of the current-current correlation function is

$$|2g_T - 1|^{\#\text{rounds}} \Leftrightarrow \exp \left[-2 \left(\frac{v_F}{\ell} \right) |t| \right] \quad (18)$$

With the identification of $\#\text{rounds}$ as $t/(L/v_F)$ we deduce that for $g_T \sim 1$ the mean free path is $\ell \approx L/(1 - g_T)$. A more detailed analysis [14] leads to the result

$$G_{\text{Drude}} = \frac{e^2}{2\pi\hbar} \sum_{a,b} [2\mathbf{g}^T / (1 - \mathbf{g}^T + \mathbf{g}^R)]_{a,b} \quad (19)$$

If the device were opened as in Fig. 1e we could ignore the multiple rounds. In such case we would obtain

$$G_{\text{Landauer}} = \frac{e^2}{2\pi\hbar} \sum_{a,b} [\mathbf{g}^T]_{a,b} \quad (20)$$

Both results, the Drude result for the closed device and the Landauer result for the corresponding open geometry, are “classical” in the sense of Boltzmann, which means that they depend only on \mathbf{g} .

Let us see what do we get for G_{Landauer} and for G_{Drude} in the case of the prototype system that we have defined in section 2. The calculation of G_{Landauer} is trivial and leads to Eq.(3). The calculation of G_{Drude} is more complicated since it involves matrix inversion. Still \mathbf{g} is sufficiently simple to allow a straightforward calculation that leads to Eq.(4). The rest of this section is devoted to the details of this calculation.

We write $\mathbf{g}_T = \tau^2 \mathbf{1}$ and $\mathbf{g}_R = \epsilon^2 \mathbf{\Upsilon}$, where τ and ϵ are defined via $g_T = \tau^2 = 1 - \mathcal{M}\epsilon^2$, and where we have introduced the following $\mathcal{M} \times \mathcal{M}$ matrices

$$\mathbf{1} = \begin{pmatrix} 1 & 0 & 0 & \cdots \\ 0 & 1 & 0 & \cdots \\ 0 & 0 & 1 & \cdots \\ \cdots & & & \cdots \\ \cdots & & & \cdots \end{pmatrix} \quad \text{and} \quad \mathbf{\Upsilon} = \begin{pmatrix} 1 & 1 & 1 & \cdots \\ 1 & 1 & 1 & \cdots \\ 1 & 1 & 1 & \cdots \\ \cdots & & & \cdots \\ \cdots & & & \cdots \end{pmatrix} \quad (21)$$

Note that the two matrices commute. Using these notations we get

$$\frac{2\mathbf{g}_T}{\mathbf{1} - \mathbf{g}_T + \mathbf{g}_R} = \frac{2\tau^2}{1 - \tau^2} \frac{1}{\mathbf{1} + \frac{\epsilon^2}{1 - \tau^2} \mathbf{\Upsilon}} \quad (22)$$

$$= \frac{2\tau^2}{1 - \tau^2} \frac{1}{\mathbf{1} + \mathbf{c}\mathbf{c}^t} = \frac{2\tau^2}{1 - \tau^2} \mathbf{1} - \frac{\epsilon^2 \tau^2}{(1 - \tau^2)^2} \mathbf{\Upsilon} \quad (23)$$

where we have defined the normalized column vector

$$\mathbf{c}_a = \frac{\epsilon}{\sqrt{1 - \tau^2}} \quad a = 1, 2, \dots, \mathcal{M} \quad (24)$$

and we have used the identity

$$\frac{1}{\mathbf{1} + \mathbf{c}\mathbf{c}^t} = \mathbf{1} - \frac{1}{1 + \mathbf{c}^t\mathbf{c}}\mathbf{c}\mathbf{c}^t = \mathbf{1} - \frac{1}{2}\mathbf{c}\mathbf{c}^t \quad (25)$$

Observing that $\sum_{ab} \mathbf{1}_{ab} = \mathcal{M}$ and $\sum_{ab} \Upsilon_{ab} = \mathcal{M}^2$ we get the desired result Eq.(4).

4. The quantum Kubo formula and beyond

Our objective is to find the conductance of the closed ring in circumstances such that the motion inside the ring is coherent (quantum interference within the bonds is not ignored). The calculation is done using the quantum version of Eq.(13) which involves the matrix elements \mathcal{I}_{nm} of the current operator:

$$G = \pi\hbar \varrho_F^2 \times \langle\langle |\mathcal{I}_{nm}|^2 \rangle\rangle \quad (26)$$

This equation would be the traditional Kubo formula if $\langle\langle \dots \rangle\rangle$ stood for a simple algebraic average over near diagonal matrix elements at the energy range of interest. By near diagonal elements we mean $|E_n - E_m| \lesssim \Gamma$, where Γ is level broadening parameter. The levels of the system are effectively “broadened” due to the non-adiabaticity of the driving [31] or due to the interaction with the noisy environment [5]. In what follows we assume

$$\Delta \ll \Gamma \ll \Delta_b \quad (27)$$

where $\Delta = 1/\varrho_F$ is the mean level spacing, and $\Delta_b = \pi\hbar v_F/L$ is the Thouless energy. (Note that $\Delta_b/\Delta = \mathcal{M}$). Contrary to the naive expectation it has been argued in [15] that depending on the physical circumstances the definition of $\langle\langle \dots \rangle\rangle$ may involve a more complicated *coarse graining* procedure. Consequently the result for G may differ by orders of magnitude from the traditional Kubo-Drude result. We shall discuss this key observation in later sections.

For a network system $\varrho_F = \mathcal{M}L/(\pi\hbar v_F)$. Furthermore it is convenient to define a scaled matrix I_{nm} via the relation

$$\mathcal{I}_{nm} = -i(ev_F/L)I_{nm} \quad (28)$$

so as to deal with real dimensionless quantities. Thus we re-write Eq.(26) as:

$$G = \frac{e^2}{2\pi\hbar} 2\mathcal{M}^2 \mathbf{g} \quad (29)$$

where $\mathbf{g} \equiv \langle\langle |I_{nm}|^2 \rangle\rangle$. In later sections we shall discuss the recipe for the \mathbf{g} calculation. It is important to realize (see next section) that $\mathbf{g} < 1$. This implies a quantum mechanical bound on G .

5. The quantum bound on G

We write the channel wavefunctions as $\Psi_a(x) = A_a \sin(kx + \varphi)$, where a labels the modes. In our simplified network model the modes are re-interpreted as bonds, and we assume that the wavevector $k = (2mE)^{1/2}$ is the same for all bonds. For the matrix elements of \mathcal{I} we have the expression

$$\mathcal{I}_{nm} \approx -iev_F \sum_a \frac{1}{2} A_a^{(n)} A_a^{(m)} \sin(\varphi_a^{(n)} - \varphi_a^{(m)}) \quad (30)$$

were the approximation takes into account that our interest is in the couplings between levels with $k_n \approx k_m \approx k_F$. From this expression we deduce that the scaled matrix elements of Eq.(28) are bounded as follows:

$$I_{nm} < \sum_a \frac{L}{2} A_a^{(n)} A_a^{(m)} < 1 \quad (31)$$

Therefore, irrespective of the details of the averaging or coarse graining procedure, it is clear that $g < 1$ as stated at the end of the previous section. Consequently

$$G \Big|_{\text{maximal}} = \frac{e^2}{2\pi\hbar} \mathcal{M}^2 \quad (32)$$

In the last expression we have omitted a factor of 2. This is not a typo. We shall explain this point in section 12.

6. The ergodic result for G

The simplest hypothesis is that all the wavefunctions are ergodic random waves. This is in the spirit of Mott's derivation [24, 25], where it has been demonstrated that a random wave assumption recovers (via Eq.(26)) the Drude result. If indeed the wavefunctions were spread equally over all the bonds, it would imply $|A_a|^2 \sim 2/(ML)$. If this were true we would get

$$|I_{nm}|^2 = \left| \frac{1}{\mathcal{M}} \sum_a \sin(\varphi^{(n)} - \varphi^{(m)}) \right|^2 \approx \frac{1}{2\mathcal{M}} \quad (33)$$

This would imply that the conductance of a ballistic (chaotic) ring is

$$G \Big|_{\text{ergodic}} = \frac{e^2}{2\pi\hbar} \mathcal{M} \quad (34)$$

We would like to argue that this result is wrong. Moreover, it must be wrong. The result is wrong because the eigenfunction of a ballistic ring are not ergodic. This we discuss in section 10. Furthermore, the result *must* be wrong because it violates quantum-classical correspondence, which we discuss in the next section.

7. The quantum conductance and Drude

In this section we define the distinction between mesoscopic and spectroscopic conductance and further discuss the latter. In the next section we elaborate on the calculation procedure of both. We would like to clarify in advance that the spectroscopic conductance is the outcome of the traditional Kubo calculation. Moreover, it is only the spectroscopic conductance which obeys quantum-classical correspondence considerations.

Mesoscopic conductance: If the environmentally induced relaxation can be neglected, the rate of energy absorption depends on having *connected* sequences of transitions between levels [15]. In the next section we explain the proper procedure for calculating the conductance in such circumstances. The result that comes out from such calculation is what we call the mesoscopic conductance G_{meso} .

Spectroscopic conductance: Within the framework of linear response theory, it is assumed that the EMF-induced transitions are very slow compared with the environmentally induced relaxation. Then one can argue that Eq.(26) is valid with

$\langle\langle |\mathcal{I}_{nm}|^2 \rangle\rangle$ interpreted as an *algebraic average* over the matrix elements. This is what we called in section 4 the *traditional* Kubo formula. Optionally, if applicable, one may perform an algebraic average over realizations of disorder. The latter is a very common procedure in diagrammatic calculations. The outcome of the (traditional) calculation is what we call the spectroscopic conductance G_{spec} . For further discussion of the conditions that justify a “spectroscopic” calculation see Ref. [15].

The spectroscopic conductance is not very sensitive to Γ . In fact the Γ dependence of the result is nothing else but the weak localization correction [12]. It scales like Δ/Γ for diffusive rings, where Δ is the mean level spacing (note Eq.(27)).

Disregarding weak localization corrections it can be argued [15] that the obtained result for G_{spec} is G_{Drude} provided some reasonable quantum-to-classical correspondence conditions (see below) are satisfied. It follows that the ergodic hypothesis of the previous section cannot be correct, because G_{Drude} is definitely not bounded by the number of open modes - it can be much larger.

The necessary condition for quantum-classical correspondence can be deduced by taking into account the quantum bound of section 5. As g_T becomes closer to 1, the Drude expression diverges. Quantum-to-classical correspondence is feasible provided the quantum bound is not exceeded:

$$\frac{1}{1 - g_T} \ll \mathcal{M} \quad (35)$$

This can be re-phrased as

$$\frac{\ell}{L} < \mathcal{M} \quad (36)$$

or as

$$t_{cl} \ll t_H \quad (37)$$

where $t_{cl} = \ell/v_F$ is the ballistic time, and $t_H = \mathcal{M} \times (L/v_F)$ is the Heisenberg time (the time to resolve the quantized energy levels). In order to establish quantum-to-classical correspondence in a constructive manner one should express the Kubo formula using Green functions, leading to a double summation over paths. Then one should argue that energy averaging justify the use of the diagonal approximations. The procedure is the same as in [32]. Needless to say that Eq.(34) is not consistent with this argued correspondence and therefore a-priori *must* be wrong.

8. The calculation of G

The SLRT recipe for the calculation of G is implied by the following statements:

- [A] The transitions rates between levels (w_{nm}) are given by the FGR.
- [B] The diffusion in energy (D) is given by a resistor network calculation.
- [C] The diffusion-dissipation relation at low temperatures is $\dot{W} = \varrho_F D$.
- [D] The expression for the conductance G is identified via Eq.(1).

In this section we give all the relevant details for using this recipe. The Hamiltonian of the ring in the adiabatic basis is $\mathcal{H} \mapsto E_n \delta_{nm} + W_{nm}$ where $W_{nm} = i\dot{\Phi} \hbar \mathcal{I}_{nm} / (E_n - E_m)$, and $-\dot{\Phi}$ is the EMF. The FGR transition rate between level n and level m is

$$w_{nm} = \frac{2\pi}{\hbar} \delta(E_n - E_m) |W_{nm}|^2 \quad (38)$$

Since we are dealing with a closed system one should take explicitly into account the broadening of the delta function:

$$\delta(E_n - E_m) \mapsto \frac{1}{\Gamma} F\left(\frac{E_n - E_m}{\Gamma}\right) \quad (39)$$

The normalized kernel $F()$ reflects either the power spectrum or the non-adiabaticity of the driving. For the purpose of numerical demonstration we assume $F(r) = \exp(-2|r|)$ as in [17]. The level broadening Γ is identical with Γ of Ref.[15, 31] and with $\hbar\omega_0$ of Ref.[17]. As in the conventional derivation of linear response theory [12], also here we regard Γ as a free parameter in the theory. It is convenient to use dimensionless quantities, so we re-write Eq.(38) as:

$$w_{nm} = \varrho_F \frac{e^2}{\pi\hbar} \mathcal{M}^2 \mathbf{g}_{nm} \dot{\Phi}^2 \quad (40)$$

where the dimensionless transition rates are

$$\mathbf{g}_{nm} = 2\varrho_F^{-3} \frac{|I_{nm}|^2}{(E_n - E_m)^2} \frac{1}{\Gamma} F\left(\frac{E_n - E_m}{\Gamma}\right) \quad (41)$$

In practice we could make the approximation $(E_n - E_m)/\Delta \approx (n - m)$, that underestimates exceptionally large couplings between almost degenerated levels. Such an approximation would not be reflected in the G_{meso} calculation (see below), because the latter is determined by the bottlenecks.

The FGR transitions between levels lead to diffusion in energy space. We would like to calculate the *coarse grained diffusion coefficient* D without assuming that all the $|I_{nm}|^2$ are comparable. For this purpose it is useful to exploit the following resistor network analogy [17]:

$$w_{nm}^{-1} \iff \text{resistor between node } n \text{ and node } m \quad (42)$$

$$D^{-1} \iff \text{resistivity of the network} \quad (43)$$

In dimensionless units w_{nm} is denoted as \mathbf{g}_{nm} as defined via Eq.(40). In dimensionless units D is denoted as \mathbf{g} and it is defined via the following equation:

$$D = \varrho_F^{-1} \frac{e^2}{\pi\hbar} \mathcal{M}^2 \mathbf{g} \dot{\Phi}^2 \quad (44)$$

The extra ϱ_F^{-2} factor compared with Eq.(40) arise because the resistivity D^{-1} is calculated per unit “energy length” while the scaled resistivity \mathbf{g}^{-1} is per unit site.

A standard numerical procedure is used for extracting \mathbf{g} for a given resistor network \mathbf{g}_{nm} . The steps are as follows: **(i)** Cut an N site segment out of the network (Fig. 3). **(ii)** Define a vector $\mathbf{J}_n (n = 1..N)$ whose elements are all zero except the first and the last that equal $\mathbf{J}_1 = +J$ and $\mathbf{J}_N = -J$. **(iii)** Solve the matrix equation

$$\mathbf{J}_n = \sum_m \mathbf{g}_{nm} (\mathbf{V}_n - \mathbf{V}_m) \quad (45)$$

This equation should be solved for \mathbf{V}_n . In practice it is easier to write this equation as $\mathbf{J} = -\tilde{\mathbf{g}}\mathbf{V}$ where $\tilde{\mathbf{g}}_{nm} = \mathbf{g}_{nm} - \delta_{nm} \sum_{m'} \mathbf{g}_{nm'}$. The difference $\mathbf{V}_1 - \mathbf{V}_N$ is obviously proportional to the injected J . **(iv)** Find the overall resistance of the truncated network $\mathbf{g}_N = J/(\mathbf{V}_N - \mathbf{V}_1)$. And finally: **(v)** Define the resistivity as $\mathbf{g}^{-1} = \mathbf{g}_N^{-1}/N$. For a locally homogeneous network it has been argued in Ref.[15] that \mathbf{g} can be obtained via an harmonic average:

$$\mathbf{g}|_{\text{meso}} \approx \left[\frac{1}{N} \sum_n \left[\frac{1}{2} \sum_m (m - n)^2 \mathbf{g}_{nm} \right]^{-1} \right]^{-1} \quad (46)$$

The internal sum reflects addition of resistors in parallel, while the harmonic average reflects addition of resistors in series. This should be contrasted with the algebraic average which is used in order to calculate the spectroscopic result:

$$\mathbf{g}\Big|_{\text{spec}} = \left[\frac{1}{N} \sum_n \left[\frac{1}{2} \sum_m (m-n)^2 \mathbf{g}_{nm} \right] \right] \quad (47)$$

It is a simple exercise to verify that if all the matrix elements are the same, say $|I_{nm}|^2 = \sigma^2$, then $\mathbf{g}_{\text{meso}} = \mathbf{g}_{\text{spec}} = \sigma^2$. But if the matrix is structured or sparse then \mathbf{g}_{meso} is much smaller compared with \mathbf{g}_{spec} . Schematically we write in both cases

$$\mathbf{g} = \langle\langle |I_{nm}|^2 \rangle\rangle \quad (48)$$

It should be clear that in both cases (spectroscopic, mesoscopic) the ‘‘averaging’’ requires the specification of the smoothing scale Γ as implied by Eq.(41). It is also clear that the mesoscopic result is much more sensitive to the value of Γ . Unlike the spectroscopic result where the dependence on Γ is merely a ‘‘weak localization correction’’ [12], in the case of the mesoscopic result the dependence on Γ is a leading order effect.

The diffusion-dissipation relation states that the rate of energy absorption is $\dot{W} = \varrho_{\text{F}} D$. Then it is implied by Eq.(1) that the conductance G is given by Eq.(29). The procedure above can be summarized by saying that \mathbf{g} can be calculated from $|I_{nm}|^2$ via an appropriate ‘‘averaging procedure’’. The appropriate averaging procedure is *algebraic* (Eq.(47)) in the case of the spectroscopic conductance. The appropriate averaging procedure is *harmonic-type* (as discussed above) in the case of mesoscopic conductance.

9. The eigenstates of the network model

The network model that we have presented in section 2 is defined in terms of the scattering matrix \mathbf{S}_{D} , and the free propagation matrix \mathbf{S}_{W} ,

$$\mathbf{S}_{\text{D}} = \begin{pmatrix} \epsilon \exp(i 2\pi \frac{ab}{M}) & \sqrt{1 - \mathcal{M}\epsilon^2} \delta_{a,b} \\ \sqrt{1 - \mathcal{M}\epsilon^2} \delta_{a,b} & -\epsilon \exp(-i 2\pi \frac{ab}{M}) \end{pmatrix} \quad (49)$$

$$\mathbf{S}_{\text{W}} = \begin{pmatrix} 0 & e^{ikL_a} \delta_{ab} \\ e^{ikL_a} \delta_{ab} & 0 \end{pmatrix} \quad (50)$$

The wavefunction can be written as

$$|\psi\rangle \mapsto \sum_{a=1}^{\mathcal{M}} \left(A_{L_a} e^{ik(x-L_a)} + A_{R_a} e^{-ikx} \right) \otimes |a\rangle. \quad (51)$$

The set of amplitudes A_L and A_R that can be arranged as a column vector of length $2\mathcal{M}$. The linear equation for the eigenstates is

$$\begin{pmatrix} A_L \\ A_R \end{pmatrix} = \mathbf{S}_{\text{W}} \mathbf{S}_{\text{D}} \begin{pmatrix} A_L \\ A_R \end{pmatrix} \quad (52)$$

and the associated secular equation for the eigenvalues is

$$\det[\mathbf{S}_{\text{W}} \mathbf{S}_{\text{D}} - 1] = 0 \quad (53)$$

In the absence of driving we have time reversal symmetry, and the unperturbed eigenfunctions can be chosen as real (see appendix A):

$$|\psi\rangle \mapsto \sum_{a=1}^{\mathcal{M}} A_a \sin(kx + \varphi_a) \otimes |a\rangle. \quad (54)$$

The wavefunction is normalized as

$$\sum_{a=1}^{\mathcal{M}} \int_0^{L_a} A_a^2 \sin^2(kx + \varphi_a) dx = 1 \quad (55)$$

which implies

$$\sum_{a=1}^{\mathcal{M}} \frac{L_a}{2} A_a^2 \approx 1 \quad (56)$$

For a given g_T we can find numerically the eigenvalues and the eigenstates, thus obtaining a table

$$(k_n, \varphi_a^{(n)}, A_a^{(n)}) \quad n = \text{level index} \quad (57)$$

For the numerical study we have chosen a network system consisting of $\mathcal{M} = 50$ bonds. The length of each bond is randomly selected in the range $L_a = 1 \pm 0.1$. We select the eigenvalues with $k_n \sim 2000$. The numerical results over the whole range of g_T values are presented in Figs. 4-7. In the following sections we discuss and analyze these results.

It is of course possible to determine analytically what are the eigenvalues and the eigenstates in the $g_T \rightarrow 1$ limit. The combined scattering matrix is

$$\mathbf{S}_W \mathbf{S}_D = \begin{pmatrix} \tau e^{ikL_a} \delta_{a,b} & -\epsilon e^{i(kL_a - \frac{2\pi}{\mathcal{M}} a \times b)} \\ \epsilon e^{i(kL_a + \frac{2\pi}{\mathcal{M}} a \times b)} & \tau e^{ikL_a} \delta_{a,b} \end{pmatrix} \quad (58)$$

where we use the notation $\tau = (1 - \mathcal{M}\epsilon^2)^{1/2}$. For $g_T = 1$ this matrix becomes diagonal. Then it has \mathcal{M} distinct eigenvalues, each doubly degenerate. We are interested in the non-degenerate case in the limit $\epsilon \rightarrow 0$. The eigenstates are still localized each in a single a bond, but the degeneracy is lifted. Within the framework of degenerate perturbation theory we have to diagonalize the 2×2 matrix

$$\begin{pmatrix} \tau e^{ikL_a} & -\epsilon e^{i(kL_a - \frac{2\pi a^2}{\mathcal{M}})} \\ \epsilon e^{i(kL_a + \frac{2\pi a^2}{\mathcal{M}})} & \tau e^{ikL_a} \end{pmatrix} \quad (59)$$

whose eigenvalue are determined by the associated secular equation

$$(\epsilon^2 + \tau^2)e^{2ikL_a} - 2\tau\epsilon e^{ikL_a} + 1 = 0 \quad (60)$$

Hence we get the following approximations

$$k_n \approx \left(2\pi \times \text{integer} \pm \frac{1}{\sqrt{\mathcal{M}}} \epsilon \right) \frac{1}{L_a} \quad (61)$$

$$\varphi_a^{(n)} \approx -\frac{a^2}{\mathcal{M}}\pi - \frac{1}{2}k_n L_a + \begin{cases} \pi/4 \\ 3\pi/4 \end{cases} \quad (62)$$

We have verified that the numerical results of Fig. 4 and Fig. 7 agree with these estimates. We note that for hard wall scatterer each φ_a would become either 0 or $\pi/2$ in the $g_T \rightarrow 1$ limit.

10. The non-ergodicity of the eigenfunctions

In Fig. 5 we display images of the column vectors $A_a^{(n)}$ for two representative values of g_T so as to illustrate the crossover from localized to ergodic wavefunctions. Each eigen-function can be characterized by its participation ratio:

$$\text{PR} = \left[\sum_a \left(\frac{L_a}{2} A_a^2 \right)^2 \right]^{-1} \quad (63)$$

This constitutes a measure for the ergodicity of the eigen-functions. By this definition

$$\text{PR} \approx \begin{cases} 1 & \text{for a single bond localized state} \\ \mathcal{M} & \text{for a uniformly distributed state} \end{cases} \quad (64)$$

We distinguish between 3 regimes depending on the value of the total transmission g_T ,

- The trivial ballistic regime $(1 - g_T) \ll 1/\mathcal{M}$ for which $\text{PR} \sim 1$
- The non-trivial ballistic regime $1/\mathcal{M} \ll (1 - g_T) \ll 1$.
- The non-ballistic regime where g_T is not close to 1 and $\text{PR} \sim \mathcal{M}$

In the trivial ballistic regime the eigenstates are like those of a reflection-less ring with uncoupled modes, hence $\text{PR} \sim 1$. Once $(1 - g_T)$ becomes larger compared with $1/\mathcal{M}$ first order perturbation theory breaks down, and the mixing of the levels is described by a Wigner Lorentzian. The analysis is completely analogous to that of the single mode case of Ref.[15], leading to $\text{PR} \propto (1 - g_T) \times \mathcal{M}$. For g_T values that are not close to 1 the eigen-functions become ergodic with $\text{PR} \sim \mathcal{M}$. From RMT we expect [33] $\text{PR} \sim \mathcal{M}/3$. A satisfactory global fit, that works well within the non-trivial ballistic regime is (Fig. 8):

$$\text{PR} \approx 1 + \frac{1}{3}(1 - g_T)\mathcal{M} \quad (65)$$

Our interest is focused in the *non-trivial* ballistic regime $1/\mathcal{M} \ll (1 - g_T) \ll 1$, where we have strong mixing of levels ($\text{PR} \gg 1$), but still the mean free path $\ell \approx L/(1 - g_T)$ is very large compared with the ring's perimeter ($\ell \gg L$). In view of the discussion in section 6, it is important to realize that in this regime we do not have “quantum chaos” ergodicity. Rather we have $\text{PR} \ll \mathcal{M}$ meaning that *the wavefunctions occupy only a small fraction of the classically accessible phase space.*

11. The calculation of matrix elements

Given a set of eigenstates, it is straightforward to calculate the matrix elements of the current operator (Figs. 9-12). We recall that the scaled matrix elements are

$$I_{nm} \approx \sum_a \frac{L_a}{2} A_a^{(n)} A_a^{(m)} \sin(\varphi_a^{(n)} - \varphi_a^{(m)}) \quad (66)$$

with the associated upper bound

$$\bar{I}_{nm} \approx \sum_a \frac{L_a}{2} A_a^{(n)} A_a^{(m)} \quad (67)$$

For $n = m$ we have $\bar{I}_{nm} = 1$ due to normalization, and $I_{nm} = 0$ due to time reversal symmetry. From now on we are interested in $n \neq m$. There are several extreme cases that allow simple estimates:

$$\bar{I}_{nm} \approx \begin{cases} 0 & \text{for pair of states localized on different bonds} \\ 1 & \text{for pair of states localized on the same bond} \\ 1 & \text{for pair of ergodic states} \end{cases}$$

If we take the phases into account we get

$$|I_{nm}|^2 \approx \begin{cases} 0 & \text{for pair of states localized on different bonds} \\ 1 & \text{for pair of nearly degenerated states on the same bond} \\ 1/(2\mathcal{M}) & \text{for pair of uncorrelated ergodic states} \end{cases}$$

We have already explained in section 6 that the “ergodic” hypothesis is wrong in the ballistic case. It should be clear that the small PR of the eigenfunctions implies sparsity of I_{nm} : The matrix elements are very small for any pair of states that are localized on different sets of bonds. This observation is demonstrated in Figs. 9-12. As the reflection $1 - g_T$ is increased, more and more elements become non-negligible, and the matrix becomes less structured and less sparse.

12. Numerical results for the conductance

Once we have the matrix elements $|I_{nm}|^2$ we can calculate G_{spec} using the algebraic average recipe Eq.(47). We can also calculate G_{meso} using either the resistor network procedure or the harmonic average approximation Eq.(46). Fig. 13 displays the results for an $\mathcal{M} = 50$ network model. The conductance goes to zero for both $g_T \rightarrow 0$ and $g_T \rightarrow 1$. The dependence on Γ is plotted in Fig. 14. The rough accuracy of the harmonic average has been verified (not displayed).

The dependence of G on the smoothing parameter Γ is easily understood if we keep in our mind the band profile which is illustrated in Fig. 10. In order to improve our intuition we show in Fig. 12 the average value of $|I_{n,n+r}|^2$ for $r = 1, 2, 3, 4, 5$ as a function of $1 - g_T$ for $r = 1, 2, 3, 4, 5$.

It should be clear that the large $r = 1$ elements originate from the pairs of almost degenerate states that were discussed in section 9. Their contribution to the spectroscopic conductance is dominant. The upper bound Eq.(32) on G is implied by the upper bound on $|I_{n,n+1}|^2$. It was already pointed out in section 11 that the maximal value $|I_{nm}| = 1$ is attained for the nearly degenerate states. The algebraic average with the interlacing vanishingly small couplings leads to the factor of 1/2 that was mentioned after Eq.(32). To avoid miss-understanding we emphasize that this *prefactor* is model specific.

On the other hand, the large $r = 1$ couplings almost do not affect the mesoscopic conductance. This is because they do not form connected sequences. Moreover, as implied by our calculation recipe, large value of Γ cannot help to overcome the bottlenecks. In order to get a classical result the environment should induce not only level broadening (which is like the $1/T_2$ rate of pure dephasing in NMR studies), but also a relaxation effect (analogous to the $1/T_1$ rate in NMR).

13. Discussion

In this paper we have studied the mesoscopic conductance of a ballistic ring with mean free path $\ell \gg L$. The specific calculation has been done for a network model, but all its main ingredients are completely *generic*. Ballistic rings with $\ell \gg L$ are not typical “quantum chaos” systems. Their eigenfunctions *are not ergodic over the whole accessible phase space*, and cannot be regarded as an extended “random wave”. Consequently the perturbation matrix \mathcal{I}_{nm} is highly structured and sparse, and we have to go beyond the Kubo formalism in order to calculate the mesoscopic conductance.

Results vs expectations: The “averaging” over the matrix elements of the current operator should be done according to the appropriate prescription: algebraic scheme for the spectroscopic conductance G_{spec} , and resistor-network scheme for the mesoscopic conductance G_{meso} . The calculation procedure implies that

$$G_{\text{meso}} < G_{\text{spec}} \leq G_{\text{Drude}} \quad (68)$$

Our original naive belief, before we started with the numerical work, was that it is feasible to get quite large G_{meso} , possibly of the order of G_{spec} . To our surprise the numerics has revealed that *typically*

$$G_{\text{meso}} < G_{\text{Landauer}} \quad (69)$$

We have pushed our numerical verification of this statement up to $\mathcal{M} = 450$ (Fig. 14b). For an optimal value of Γ , such that G_{meso} is maximal, we still have $G_{\text{meso}} \lesssim G_{\text{Landauer}}$. The numerical prefactor in the latter inequality appears to be roughly 3, but obviously we cannot establish that there is a strict limitation. Still, as far as order of magnitude estimates are concerned, our conjecture is that this statement is true *in general*. We did not find a mathematical argument to establish this conjecture, except the very simple case of a single mode ballistic ring[15] where the calculations of G can be done analytically.

Robustness: Our results are not sensitive to the details of the model. Disregarding the details, the eigenfunctions are doomed to be non-ergodic in mode space if $g_T \sim 1$. This by itself implies that I_{nm} is sparse and possibly structured. Consequently the resistor network picture implies that G_{meso} is much smaller compared with the naive expectation. We have further tested the generality of our quantitative statements by analyzing [28] another, more realistic model, where the ring is modeled as a waveguide with a semi-disc scatterer (Fig. 2b). The \mathbf{S} matrix for this model is known [29, 30]. In particular we have verified that the participation ratio of the eigenstates has roughly the expected dependence on g_T . Indeed for both the semi-disc model, and our simplified network model, the participation ratio does not exhibit anomalous saturation as typical, say, for a “star graph” [34]. Eventually we have verified that the results for the mesoscopic conductance of the semi-disc model are similar to those that were obtained for the network model.

Challenges: It is still an open challenge to derive an estimate for the mesoscopic conductance in terms of g_T . It was possible to derive such an expression in the single mode case. There we have found that $G_{\text{meso}} \propto (1 - g_T)^2 g_T$. In the general case ($\mathcal{M} > 1$) the calculation is more complicated. We suspect that our expression for the participation ratio Eq.(65) constitutes an important step towards this goal. In any case we were not able to derive a reliable closed analytical expression.

Limitations: It should be emphasized that if there is either a very effective relaxation or decoherence process, then the semi-linear response theory that we have

discussed do not apply. In the presence of strong environmental influence one can justify, depending on the *circumstances* [14], either the use of the traditional Kubo-Drude result, or the use of the Landauer result.

Appendix A. Implications of time reversal symmetry

We can decompose the eigenstate equation as follows:

$$\begin{pmatrix} B_{La} \\ B_{Ra} \end{pmatrix} = S_D \begin{pmatrix} A_{La} \\ A_{Ra} \end{pmatrix} \quad (\text{A.1})$$

$$\begin{pmatrix} A_{La} \\ A_{Ra} \end{pmatrix} = S_W \begin{pmatrix} B_{La} \\ B_{Ra} \end{pmatrix} \quad (\text{A.2})$$

Above B_{La} and B_{Ra} are the amplitudes of the outgoing waves from $x = 0$, while A_{La} and A_{Ra} are the amplitudes of the ingoing waves. Conventional time-reversal-symmetry implies that both $\psi(x)$ and its complex-conjugate $\psi(x)^*$ satisfy the same Schrödinger equation. Complex conjugation turns out the incoming wave into outgoing one and vice versa, and therefore

$$\begin{pmatrix} A_{La}^* \\ A_{Ra}^* \end{pmatrix} = S_D \begin{pmatrix} B_{La}^* \\ B_{Ra}^* \end{pmatrix} \quad (\text{A.3})$$

$$\begin{pmatrix} B_{La}^* \\ B_{Ra}^* \end{pmatrix} = S_W \begin{pmatrix} A_{La}^* \\ A_{Ra}^* \end{pmatrix} \quad (\text{A.4})$$

It is not difficult to see that the two sets of equations are equivalent provided

$$S_D^{\text{transposed}} = S_D \quad (\text{A.5})$$

$$S_W^{\text{transposed}} = S_W \quad (\text{A.6})$$

If we have this (conventional) time reversal symmetry, the unperturbed eigenfunctions can be chosen as real in position representation:

$$|\psi\rangle = \sum_{a=1}^{\mathcal{M}} A_a \sin(kx + \varphi_a) \otimes |a\rangle. \quad (\text{A.7})$$

where

$$A_a = 2|A_{La}| = 2|A_{Ra}| \quad (\text{A.8})$$

$$\varphi_a = \frac{1}{2} (\pi + \arg(A_{La}/A_{Ra}) - kL_a) \quad (\text{A.9})$$

Acknowledgments

YE thanks Itamar Sela for his help to correct a subtle numerical error: some data points in the original numerical work of Ref.[27] were distorted. Much of the motivation for this work came from intriguing meetings of DC during 2004-2005 with Michael Wilkinson, who highlighted the open question regarding the feasibility to get $G > G_{\text{Landauer}}$ in the case of a multimode closed ring. We also thank Bernhard Mehlig, Tsampikos Kottos and Holger Schanz for inspiring discussions. The research was supported by the Israel Science Foundation (grant No.11/02) and by a grant from the DIP, the Deutsch-Israelische Projektkooperation.

References

- [1] M. Büttiker, Y. Imry and R. Landauer, Phys. Lett. **96A**, 365 (1983).
- [2] R. Landauer and M. Büttiker, Phys. Rev. Lett. **54**, 2049 (1985).
- [3] M. Büttiker, Phys. Rev. B **32**, 1846 (1985).
- [4] M. Büttiker, Annals of the New York Academy of Sciences, 480, 194 (1986).
- [5] by Y. Imry and N.S. Shiren, Phys. Rev. B **33**, 7992 (1986).
- [6] N. Trivedi and D. A. Browne, Phys. Rev. B **38**, 9581 (1988).
- [7] Y. Gefen and D. J. Thouless, Phys. Rev. Lett. **59**, 1752 (1987).
- [8] M. Wilkinson, J. Phys. A **21** (1988) 4021.
- [9] M. Wilkinson and E.J. Austin, J. Phys. A **23**, L957 (1990).
- [10] B. Reulet and H. Bouchiat, Phys. Rev. B **50**, 2259 (1994).
- [11] A. Kamenev, B. Reulet, H. Bouchiat, and Y. Gefen, Europhys. Lett. **28**, 391 (1994).
- [12] For a review see “(Almost) everything you always wanted to know about the conductance of mesoscopic systems” by A. Kamenev and Y. Gefen, Int. J. Mod. Phys. **B9**, 751 (1995).
- [13] Measurements of conductance of closed diffusive rings are described by B. Reulet M. Ramin, H. Bouchiat and D. Mailly, Phys. Rev. Lett. **75**, 124 (1995).
- [14] D. Cohen and Y. Etzioni, J. Phys. A **38**, 9699 (2005).
- [15] D. Cohen, T. Kottos and H. Schanz, J. Phys. A **39**, 11755 (2006).
- [16] The term “semi-linear response” to describe the outcome of the theory of Ref.[15] has been coined in a subsequent work [17] where it has been applied to the analysis of the absorption of low frequency radiation by metallic grains.
- [17] M. Wilkinson, B. Mehlig and D. Cohen, Europhysics Letters **75**, 709 (2006).
- [18] A. Miller and E. Abrahams, Phys. Rev. **120**, 745 (1960).
- [19] A. Silva and V.E. Kravtsov, cond-mat/0611083.
- [20] Private communication of DC with Alessandro Silva.
- [21] D. Cohen, cond-mat/0611663.
- [22] V. Ambegaokar, B. Halperin, J.S. Langer, Phys. Rev. B **4**, 2612 (1971).
- [23] M. Pollak, J. Non-Cryst. Solids **11**, 1 (1972).
- [24] N.F. Mott, Phil. Mag. **22**, 7 (1970).
- [25] N.F. Mott and E.A. Davis, Electronic processes in non-crystalline materials, (Clarendon Press, Oxford, 1971).
- [26] D. Stone and A. Szafer, <http://www.research.ibm.com/journal/rd/323/ibmrd3203I.pdf>
- [27] S. Bandopadhyay, Y. Etzioni and D. Cohen, Europhysics Letters **76**, 739 (2006).
- [28] Y. Etzioni, *Conductance of multimode ballistic rings*, MSc thesis, Ben-Gurion University, Beer-Sheva (2006).
- [29] R. Blümel and U.Smilansky, Physica D **36** 111 (1989).
- [30] H. Schanz and U. Smilansky, Chaos, Solitons & Fractals **5**, 1289 (1995).
- [31] The Γ issue is discussed in Section VIII of D. Cohen, Phys. Rev. B **68**, 155303 (2003).
- [32] D. Cohen, T. Kottos and H. Schanz, Phys. Rev. E **71**, 035202(R) (2005).
- [33] F.M.Izrailev, T.Kottos and G.P.Tsironis, J.Phys. C **8**, 2823 (1996).
- [34] H. Schanz and T. Kottos, Phys. Rev. Lett. **90**, 234101 (2003).

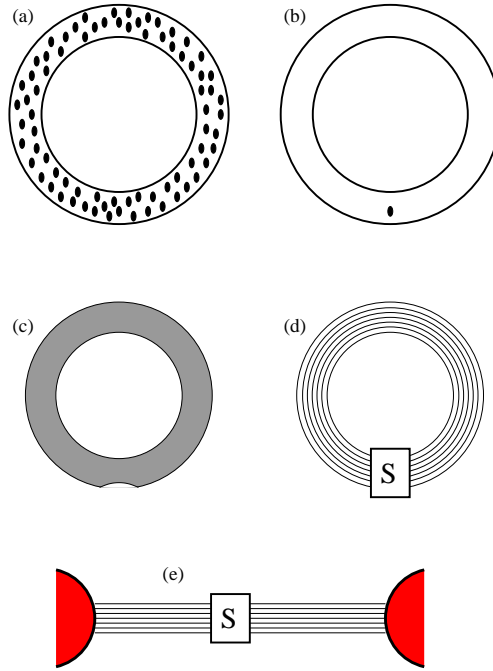


Fig.1: (a) A ring with disorder. The mean free path can be either $\ell \ll L$ for diffusive ring or $\ell \gg L$ for ballistic ring, where L is the length of the ring. (b) A chaotic ballistic ring. Here we have a single scatterer. The annular region supports \mathcal{M} open modes. (c) Another version of a chaotic ring. Here the scattering is due to a deformation of the boundary. (d) A chaotic ring can be regarded as a network. Namely, each bond corresponds to an open mode. In the numerics the lengths of the bonds ($0.9 < L_a < 1.1$) are chosen in random. The scattering is described by an S matrix. (e) The associated open (leads) geometry which is used in order to define the S matrix and the Landauer conductance.

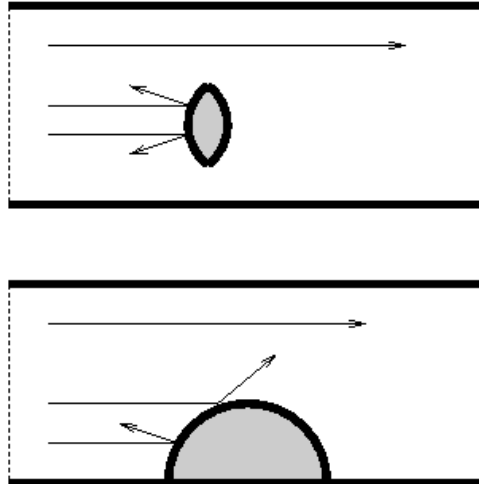


Fig.2: (a) upper panel: a waveguide with convex scatterer. This geometry has inspired our simple network model. (b) lower panel: the semi disc model. For this geometry we have some preliminary numerical results that will be published elsewhere.

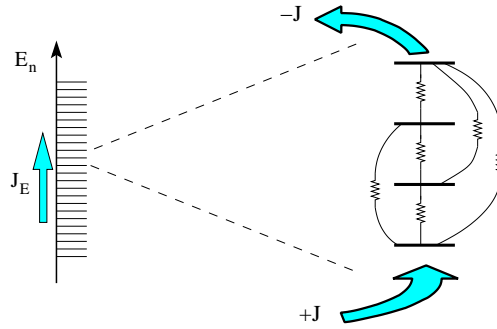


Fig.3: Within the framework of the Fermi golden rule picture the flow of the probability current in a multi level system is analogous to the flow of current via a resistor network. Thus the inverse of the coarse grained diffusion coefficient can be re-interpreted as the resistivity of the network. On the right we display a truncated segment, where $+J$ is the current injected from one end of the network, while $-J$ is the same current extracted from the other end. The injected current to all other nodes is zero. The resistance of each “resistors” in the network corresponds to g_{nm}^{-1} .

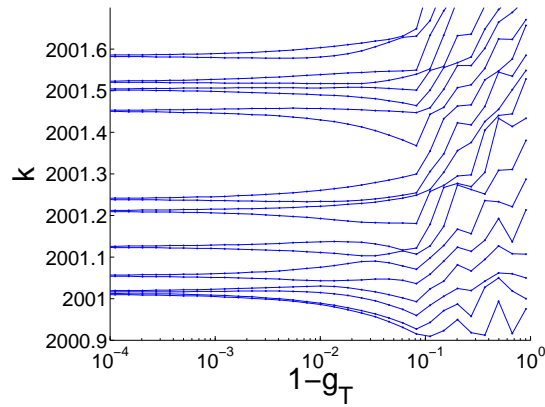


Fig.4: The eigenvalues k_n within a small energy window around $k \sim 2000$ are shown as a function of the reflection $1 - g_T$. We consider here a network model with $\mathcal{M} = 50$ bonds. The length of each bond was chosen in random within $0.9 < L_a < 1.1$.

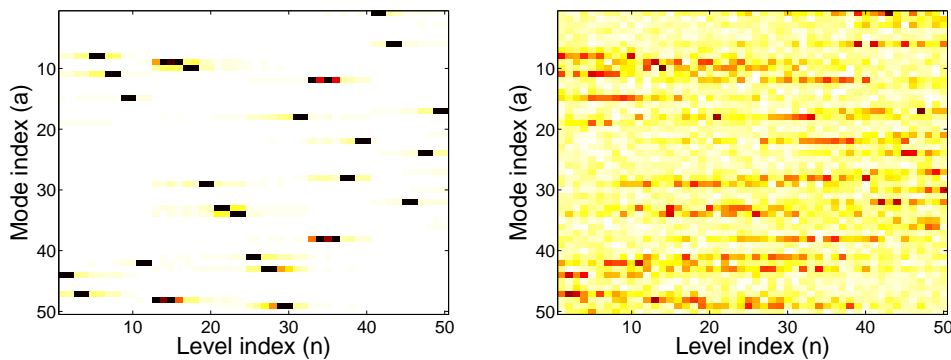


Fig.5: Each column is a grey-level image of one eigenvector $|A_a^{(n)}|^2$, where $a = 1 \dots \mathcal{M}$ is the bond index. We display the eigenvectors in the range $2000 < k < 2031$. Left panel: $g_T = 0.999$. Right panel: $g_T = 0.5$.

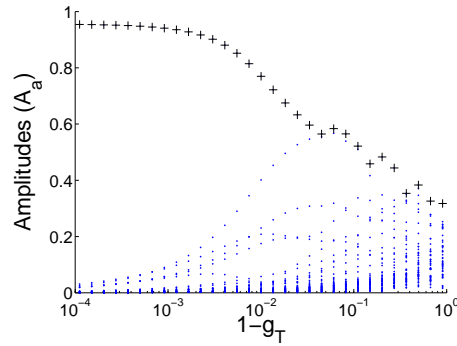


Fig.6: The amplitudes $|A_a^{(n)}|^2$ with $a = 1 \dots \mathcal{M}$ of one representative state ($k_n \approx 2011$) as a function of the reflection. The wavefunction is localized on a single bond for small reflection, and becomes ergodic for large reflection.

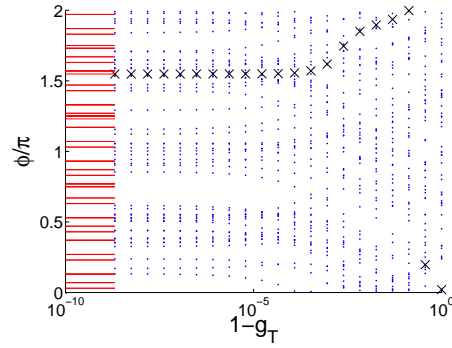


Fig.7: The phases $\varphi_a^{(n)}$ for the same eigenstate of Fig. 6. The solid lines are the values which are implied by Eq.(62). The crosses indicate the phases within the bond a where most of the wavefunction is localized. Indeed in the limit $g_T \rightarrow 1$ this phase coincides with one of the predicted values.

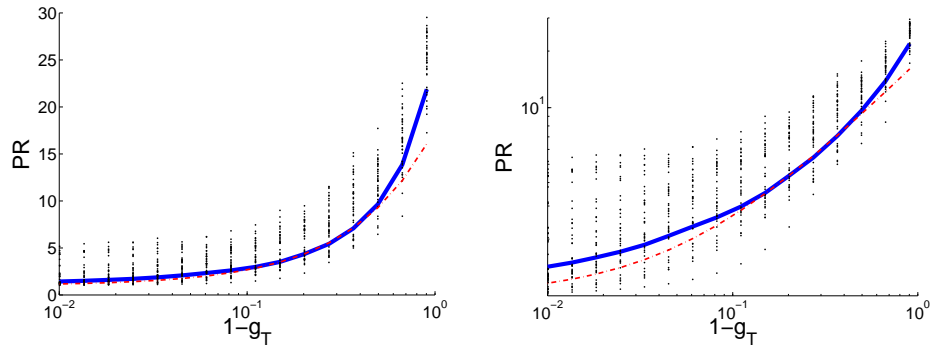


Fig.8: For each value of g_T we calculate the participation ratio (PR) for all the eigenstates. We display (as symbols) the minimum value, the maximum value, and a set of randomly chosen representative values. The solid line is the average PR, while the dotted line is Eq.(65). The left panel is log-linear while the right is log-log.

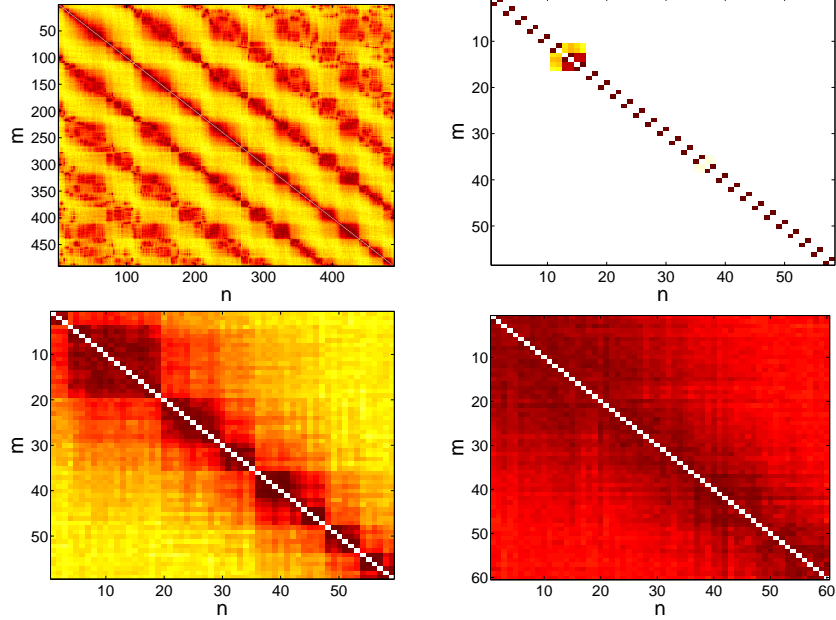


Fig.9: Images of $|\bar{I}_{nm}|^2$. The main diagonal is eliminated from the image. In left upper panel we display a relatively large representative piece for $g_T = 0.9$. In the other panels we display zoomed images for $g_T = 0.999, 0.9, 0.5$. As the reflection $1 - g_T$ becomes larger, more elements become non-negligible, and the matrix becomes less structured and less sparse.

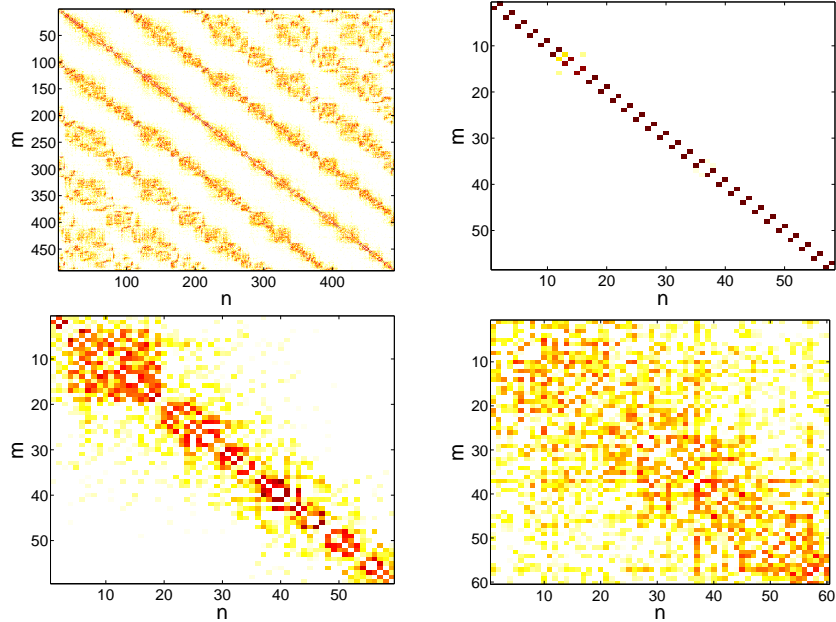


Fig.10: Images of $|I_{nm}|^2$. The main diagonal is zero due to time reversal symmetry. In left upper panel we display a relatively large representative piece for $g_T = 0.9$. In the other panels we display zoomed images for $g_T = 0.999, 0.9, 0.5$. As the reflection $1 - g_T$ becomes larger, more elements become non-negligible, and the matrix becomes less structured and less sparse.

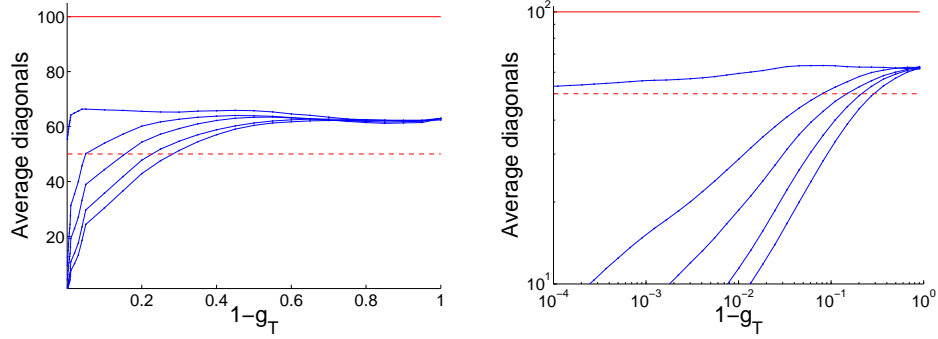


Fig.11: The n -averaged value of $2\mathcal{M}|\bar{I}_{n,n+r}|^2$ as a function of $1-g_T$ for $r = 1, 2, 3, 4, 5$. The ergodic value for this quantity ($2\mathcal{M}$) is indicated by the solid horizontal line. We also indicate the value \mathcal{M} by a dashed horizontal line. The left panel is normal scale, while the right panel is log-log.

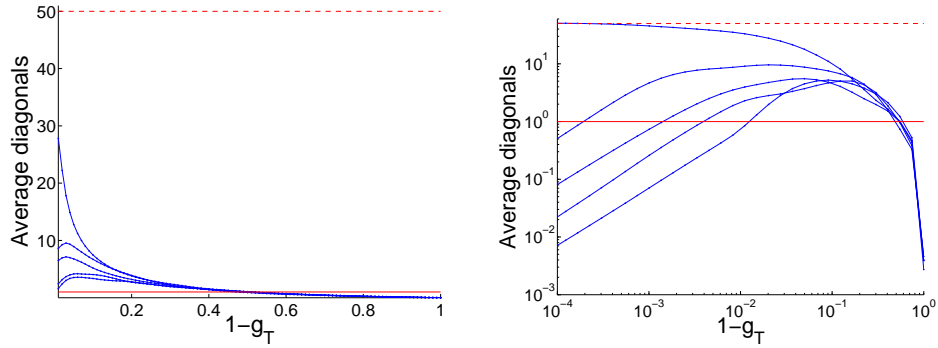


Fig.12: The n -averaged value of $2\mathcal{M}|I_{n,n+r}|^2$ as a function of $1-g_T$ for $r = 1, 2, 3, 4, 5$. The ergodic value for this quantity (1) is indicated by the solid horizontal line. We also indicate the maximal value \mathcal{M} by a dashed horizontal line. The left panel is normal scale, while the right panel is log-log.

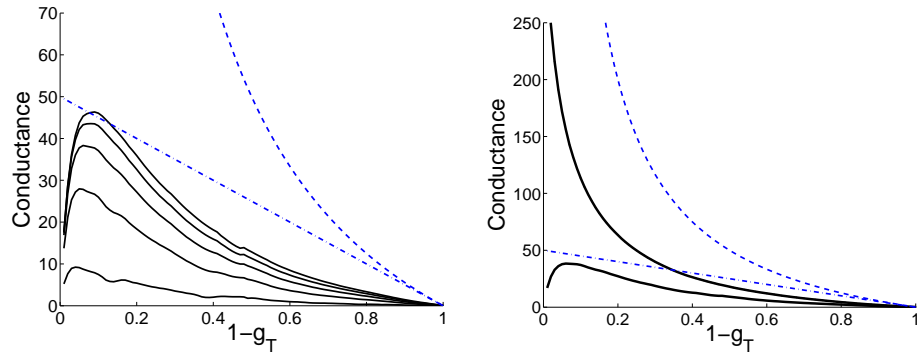


Fig.13: (a) Left panel: The mesoscopic conductance G in units of $e^2/(2\pi\hbar)$ as a function of $1-g_T$. The curves from bottom to top are for $\gamma \equiv \Gamma/\Delta = 1, 2, 3, 4, 5$. The total number of open modes is $\mathcal{M} = 50$. The dotted line is G_{Landauer} while the dashed line is G_{Drude} . (b) Right panel: The mesoscopic conductance (lower solid line) is compared with the spectroscopic conductance (upper solid line). Here $\gamma = 3$. The dotted and the dashed lines are as in the left panel.

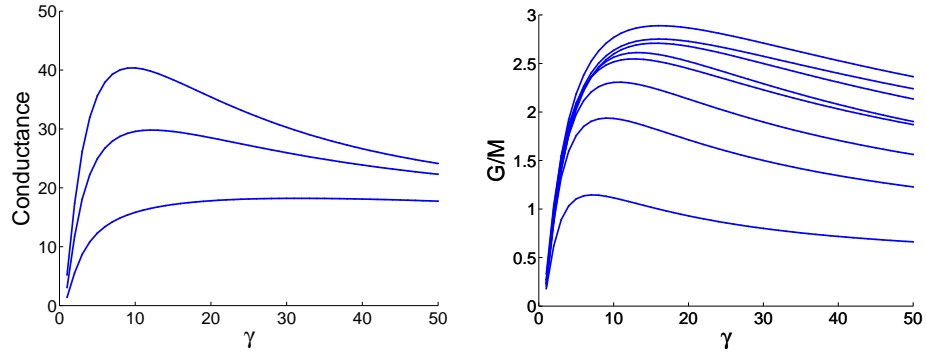


Fig.14: (a) Left panel: The mesoscopic conductance as a function of $\gamma \equiv \Gamma/\Delta$. The curves from top to bottom are for $g_T = 0.8, 0.7, 0.5$. The number of open modes is $\mathcal{M} = 50$. (b) Right panel: The mesoscopic conductance divided by the number of modes for $g_T = 0.8$ and $\mathcal{M} = 50, 100, 150, 200, 250, 300, 350, 400, 450$.